Probing enhanced superconductivity in van der Waals polytypes of VxTaS2

N.B. When citing this work, cite the original published paper.

(article starts on next page)

Probing enhanced superconductivity in van der Waals polytypes of V$_x$TaS$_2$

Wojciech R. Pudelko [1,2,*] Huanlong Liu,[2] Francesco Petocchi,[3,4] Hang Li,[1] Eduardo Bonini Guedes,[1] Julia Küspert,[2]
Karin von Arx,[2,5] Qisi Wang,[2,6] Ron Cohn Wagner,[2] Craig M. Polley,[7] Mats Leandersson,[7] Jacek Osiecki,[7]
Balasubramanian Thiagarajan,[7] Milan Radović,[1] Philipp Werner,[3] Andreas Schilling,[2]
Johan Chang,[2] and Nicholas C. Plumb[1,†]

[1]*Swiss Light Source, Paul Scherrer Institut, Forschungsstrasse 111, CH-5232 Villigen, Switzerland*
[2]*Physik-Institut, Universität Zürich, Winterthurerstrasse 190, CH-8057 Zürich, Switzerland*
[3]*Department of Physics, University of Fribourg, CH-1700 Fribourg, Switzerland*
[4]*Department of Quantum Matter Physics, University of Geneva, 24 Quai Ernest Ansermet, CH-1211 Geneva, Switzerland*
[5]*Department of Physics, Chalmers University of Technology, SE-412 96 Göteborg, Sweden*
[6]*Department of Physics, The Chinese University of Hong Kong, Shatin, Hong Kong, China*
[7]*MAX IV Laboratory, Lund University, 221 00 Lund, Sweden*

Layered transition metal dichalcogenides (TMDs) stabilize in multiple structural forms with profoundly distinct and exotic electronic phases. Interfacing different layer types is a promising route to manipulate TMDs' properties, not only as a means to engineer quantum devices but also as a route to explore fundamental physics in complex matter. Here we use angle-resolved photoemission (ARPES) to investigate a strong layering-dependent enhancement of superconductivity in TaS$_2$, in which the superconducting transition temperature, T_c, of its $2H$ structural phase is nearly tripled when insulating $1T$ layers are inserted into the system. The study is facilitated by a vanadium-intercalation approach to synthesizing various TaS$_2$ polytypes, which improves the quality of the ARPES data while leaving key aspects of the electronic structure and properties intact. The spectra show the clear opening of the charge density wave gap in the pure $2H$ phase and its suppression when $1T$ layers are introduced to the system. Moreover, in the mixed-layer $4Hb$ system, we observe a strongly momentum-anisotropic increase in electron-phonon coupling near the Fermi level relative to the $2H$ phase. Both phenomena help to account for the increased T_c in mixed $2H/1T$ layer structures.

I. INTRODUCTION

Layered transition metal dichalcogenides (TMDs) are quasi-two-dimensional materials with rich phase diagrams involving numerous exotic electronic phases. Tantalum disulfide is a widely studied TMD, whose properties are emblematic of many compounds in this family. It typically stabilizes in one of two structural phases, $2H$ or $1T$. While chemically equivalent, these phases exhibit markedly different electronic properties. The former is a good metal, which enters a charge density wave (CDW) phase at 78 K and becomes a superconductor below 0.8 K [1]. The latter is insulating and undergoes multiple CDW transitions: incommensurate at 543 K to nearly commensurate at 352 K to fully commensurate (CCDW) below 183 K [2]. In the CCDW phase, the reconstructed unit cell forms a Star-of-David (SoD) cluster, consisting of

13 Ta atoms [3], which has been proposed to host a quantum spin liquid [4,5]. Despite the two-dimensional character of $1T$-TaS$_2$, many theoretical and experimental studies have shown non-negligible out-of-plane dispersion [6] or stacking dependence [7,8], which can further influence its electronic properties and change the gap character from band to Mott insulator [3,9,10].

Due to the delicate balance of interactions, the properties of many TMDs are highly sensitive to minute changes in virtually any material or external parameter, allowing one to, e.g., tune metal-insulator transitions [11], manipulate magnetic interactions [12], or induce or enhance superconductivity [13–18]. In addition to these diverse tunable properties, the weak couplings between layers make TMDs an especially attractive platform for engineering exotic electronic phenomena at their interfaces and manufacturing novel quantum devices [19–23].

One testament to the promise of interfacing various TaS$_2$ structures is the $4Hb$ phase, a polytype consisting of $1T$ and $1H/1H'$ elements (half-layers of the $2H$ structure) stacked alternately along the c axis [24,25]. This structure has recently attracted attention, due to evidence that it hosts a chiral superconducting state [25–27]. At the same time, the superconducting T_c of the $4Hb$ phase (2.2 K) is nearly triple that of $2H$-TaS$_2$. These observations suggest that investigations of
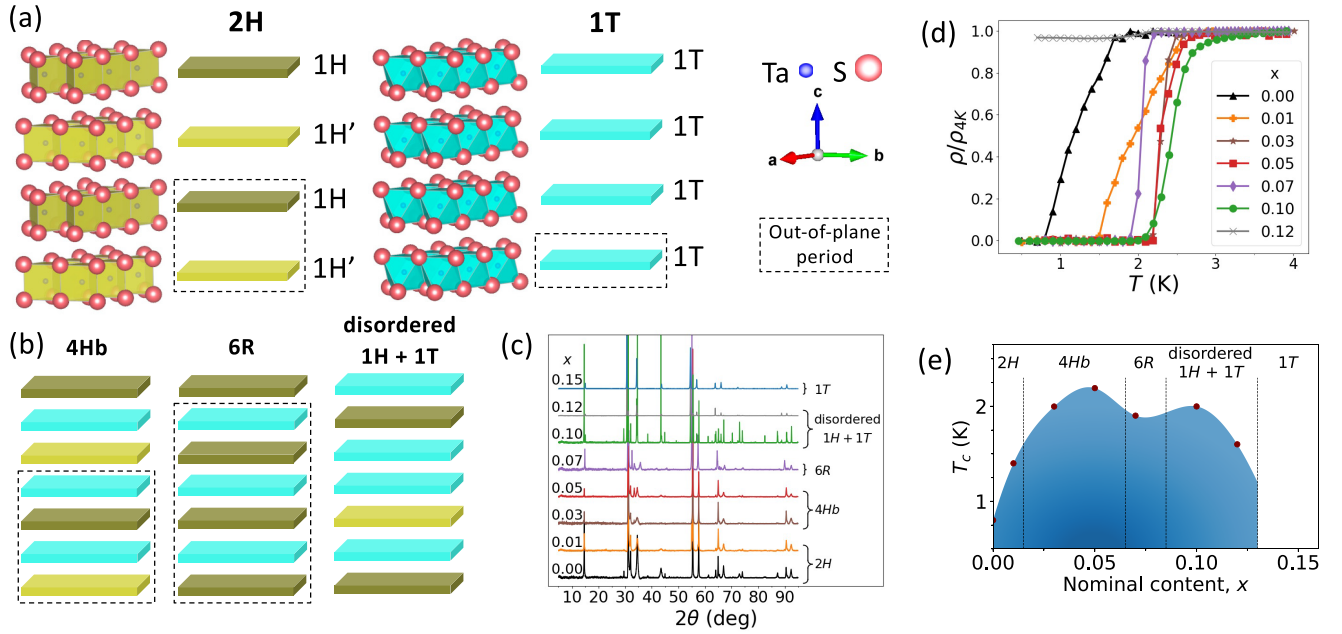
FIG. 1. (a) Crystal structures of $2H$- and $1T$-TaS$_2$. (b) Illustrations of how the $4Hb$, $6R$, and disordered phases are composed of the $2H$ ($1H$/$1H'$) and $1T$ layer elements. (c) Powder XRD measurements of V$_x$TaS$_2$ indicating changes in the structure as a function of x. (d) Normalized resistivity ρ/ρ_{4K} of V$_x$TaS$_2$ for various x values. (e) T_c as a function of x.

mixed $2H$/$1T$-TaS$_2$ layer systems can yield profound insights into the interplay of superconductivity with topology, dimensionality, many-body interactions, and competing orders.

This work investigates the strong enhancement of T_c in $4Hb$ and other mixed-layer phases of TaS$_2$. We use angle-resolved photoemission spectroscopy (ARPES) to probe the electronic structure of various polytypes of TaS$_2$. Our study utilizes vanadium intercalation to obtain the different TaS$_2$ structural configurations. We find that V$_x$TaS$_2$ samples grant clearer ARPES spectra than conventionally grown TaS$_2$ samples of the same polytypes, while possessing quantitatively similar band structures [2,28] and the same key electronic behaviors, including—most importantly—the same elevated T_c in the $4Hb$ phase relative to the $2H$ phase.

The ARPES measurements focus on the $2H$, $4Hb$, and $1T$ phases in order to identify factors at play in the strong enhancement of superconductivity in $4Hb$ and other mixed $2H$/$1T$-TaS$_2$ systems. Our results show that when $1T$ layers are inserted into the $2H$ structure, as in the $4Hb$ phase, the CDW within the $1H(')$ layers is suppressed while electron-phonon (e-ph) interactions are strongly enhanced. Surprisingly, this enhancement in electron-phonon coupling (EPC) is highly anisotropic in momentum space and only manifests in certain regions of the band structure.

II. RESULTS

Figure 1 presents an overview of the V$_x$TaS$_2$ system. The $2H$ and $1T$ layer components and their arrangements in various polytype structures are illustrated in Fig. 1(a). Data from powder x-ray diffraction (XRD) performed on samples with various x values are shown in Fig. 1(b), with labels indicating phases interpreted using standard structural data. Below $x = 0.03$, V$_x$TaS$_2$ stabilizes in the $2H$ phase. Samples

synthesized in the range of about $0.03 \leqslant x \leqslant 0.05$ have the $4Hb$ structure. In a narrow intercalation window near $x = 0.07$, the structure is assigned to the $6R$ phase. At slightly higher x levels, the arrangement of $1H(')$ and $1T$ layers appears to be disordered. Finally, at $x = 0.15$ the compound is in the pure $1T$ phase. Differences in the in-plane lattice constants of V-intercalated and conventional TaS$_2$ samples are well below 1%. Larger interlayer spacings (up to 2%) may be notable, though, particularly as they might promote cleaner sample cleavage and thereby account for the improvements in the quality of ARPES data [29]. The XRD analysis is consistent with core-level spectroscopy results, which identify distinct chemical environments of the Ta and S atoms in the $1H(')$ and $1T$ layers [29].

As shown in Fig. 1(d), a superconducting transition occurs in all samples that contain $1H$ structural components. Intercalating vanadium into the $2H$ ($x = 0$) system, and thereby inserting $1T$ layers into the structure, increases the T_c. The T_c reaches a maximum of 2.2 K in the $4Hb$ structure ($x = 0.05$), which matches the T_c in other $4Hb$-TaS$_2$ samples [25]. Further details about the structure and transport properties of the V$_x$TaS$_2$ samples are provided in the Supplemental Material (SM) [29].

Figures 2(a)–2(c) show ARPES momentum maps in the surface k_x-k_y plane, evaluated 100 meV below E_F for the $x = 0$, 0.05, and 0.15 samples. The electronic structures of the $x = 0$ and 0.15 samples are consistent with results reported for the $2H$ and $1T$ structures, respectively [2,3,30,31]. The $2H$ phase [Fig. 2(a)] is a metallic system consisting of two so-called "barrel"-shaped Fermi surface (FS) sheets centered around the Γ and K points, plus a "dogbone" sheet located at the M point [30,32], labeled as $2H$-B and $2H$-D, respectively. The $1T$ phase [Fig. 2(b)] is composed of a single gapped band that, when viewed at the energy of the gap, forms a "flower
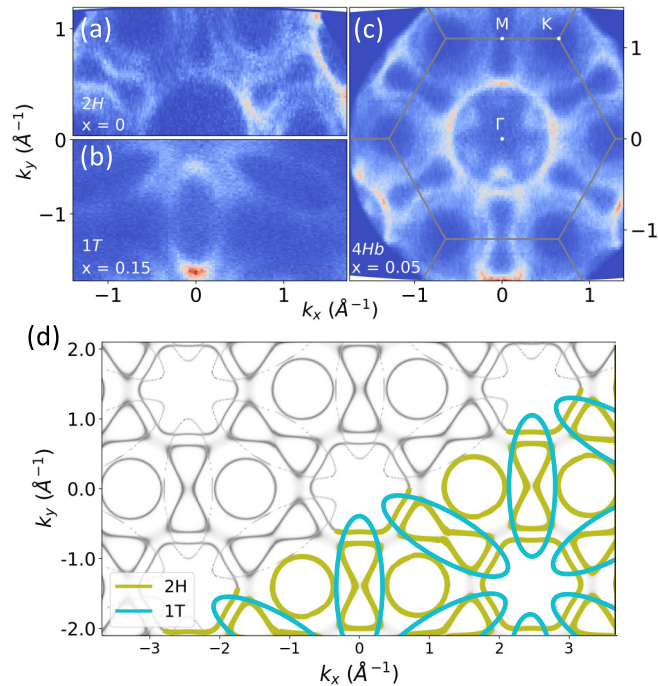
FIG. 2. (a)–(c) ARPES k-space maps evaluated at $E - E_F = -100$ meV obtained from $2H$ ($x = 0$), $1T$ ($x = 0.15$), and $4Hb$ ($x = 0.05$) samples, respectively. (d) DMFT calculation of a $2H + 1T$ model system, evaluated at $E - E_F = -100$ meV. The overlaid contours indicate contributions of the $2H$ and $1T$ components, which are evident in panel (c).

FIG. 3. (a) ARPES measurements of electron dispersions in $2H$, $4Hb$, mixed $1H + 1T$, and $1T$ samples with the noted x values. Barrel, dogbone, and flower-petal bands are labeled as $2H$-B, $2H$-D, and $1T$-FP, respectively. Rectangles in the spectra of the $2H$ and $4Hb$ samples highlight regions that are analyzed in detail in Fig. 4. (b) ARPES k_x-k_z maps of $4Hb$ and $1T$ samples, evaluated 100 meV below E_F. (c) Bulk and surface Brillouin zones. For simplicity, the "prime" notation of the surface Brillouin zone labels is dropped when considering in-plane results.

petal" in the k_x-k_y plane centered around M ($1T$-FP). In the $x = 0.05$ sample [Fig. 2(c)], spectral features originating from both the $2H$ and the $1T$ phases are visible, consistent with data reported on $4Hb$-TaS$_2$ [25]. The contributions of the $2H$ and $1T$ components to the band structure of the mixed-layer phases are highlighted by density mean-field theory (DMFT) calculations, which consider a $1T$ layer inserted into the $2H$ structure. Unlike density functional theory, the DMFT method accounts for a Hubbard interaction energy, U, within the $1T$ layers. The model results, shown in Fig. 2(d), are in reasonable agreement with the ARPES data from the $4Hb$ ($x = 0.05$) phase when assuming $U = 0.4$ eV, similar to the $1T$ system [9].

Figure 3(a) shows the evolution of the band dispersions in V$_x$TaS$_2$ with increasing x. The top left panel displays the $2H$ ($x = 0$) phase, consisting of $2H$-B and $2H$-D bands. The $1T$ ($x = 0.15$) phase, consisting of the $1T$-FP band, is shown in the bottom right panel. In the mixed $4Hb$ ($x = 0.05$) and $1H + 1T$ ($x = 0.1$) systems, all three bands are visible. While the most salient features of the $2H$- and $1T$-derived bands are preserved in these phases, there are notable differences among the spectra, which could be points of future investigation. These include a large downward shift in the energy of the $2H$ valence bands around Γ, and faint replicas of the $1T$-FP band in the $4Hb$ phase. In addition, compared to the pure $2H$ ($x = 0$) phase, the $4Hb$ ($x = 0.05$) and disordered $1H + 1T$ ($x = 0.1$) structures show a slight upward shift of the $2H$-B and -D conduction bands. The corresponding changes in Fermi momenta appear consistent with a recent observation
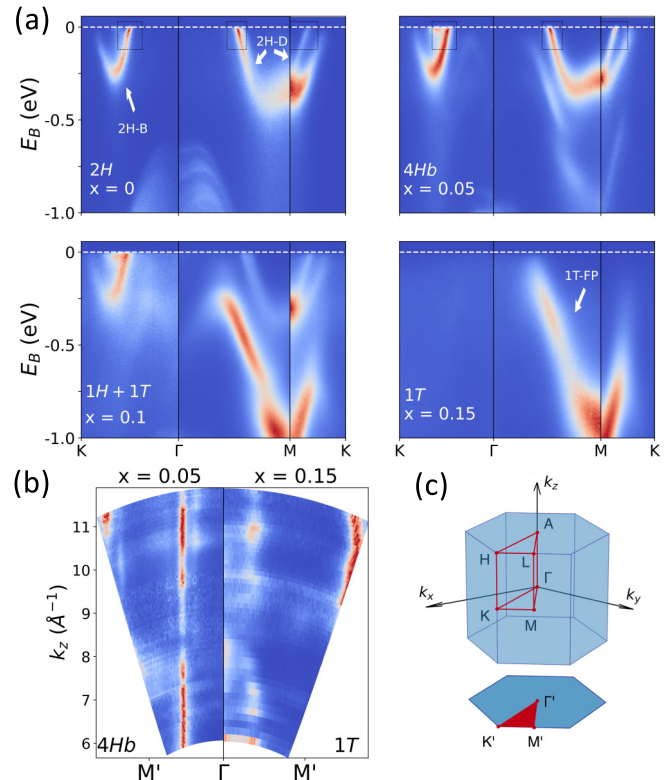
of charge transfer between the $1T$ and $1H(')$ layers within $4Hb$-TaS$_2$ [28].

We also note that, although we observe signatures of SoD reconstruction in $1T$-V$_x$TaS$_2$ ($x = 0.15$), its ARPES spectrum does not exhibit a shallow, gapped spectral feature at Γ, which is seen in conventionally grown $1T$ samples and widely ascribed to a Mott gap [6,7,33]. The lack of this feature is attributable to a difference in the vertical stacking alignment of layers [3,7,9]. As the "Mott gap" feature does not carry over into the $4Hb$ system where we investigate the enhancement of T_c [25,28], its absence in $1T$-V$_x$TaS$_2$ does not affect the current study.

Varying the photon energy in ARPES allows the electronic structure to be probed as a function of the out-of-plane momentum, k_z. Figure 3(b) compares momentum maps from the $x = 0.05$ ($4Hb$, left) and 0.15 ($1T$, right) samples in the k_x-k_z plane, evaluated 100 meV below E_F. Here the $1T$-FP band in the $x = 0.15$ sample exhibits weak but observable momentum dependence along k_z, similar to previous reports [10,34–39]. By contrast, the same $1T$-derived bands in the $4Hb$ ($x = 0.05$) phase show little to no variation with respect to k_z, signaling enhanced two-dimensionality. For orientation, the bulk and surface Brillouin zones are sketched in Fig. 3(c).
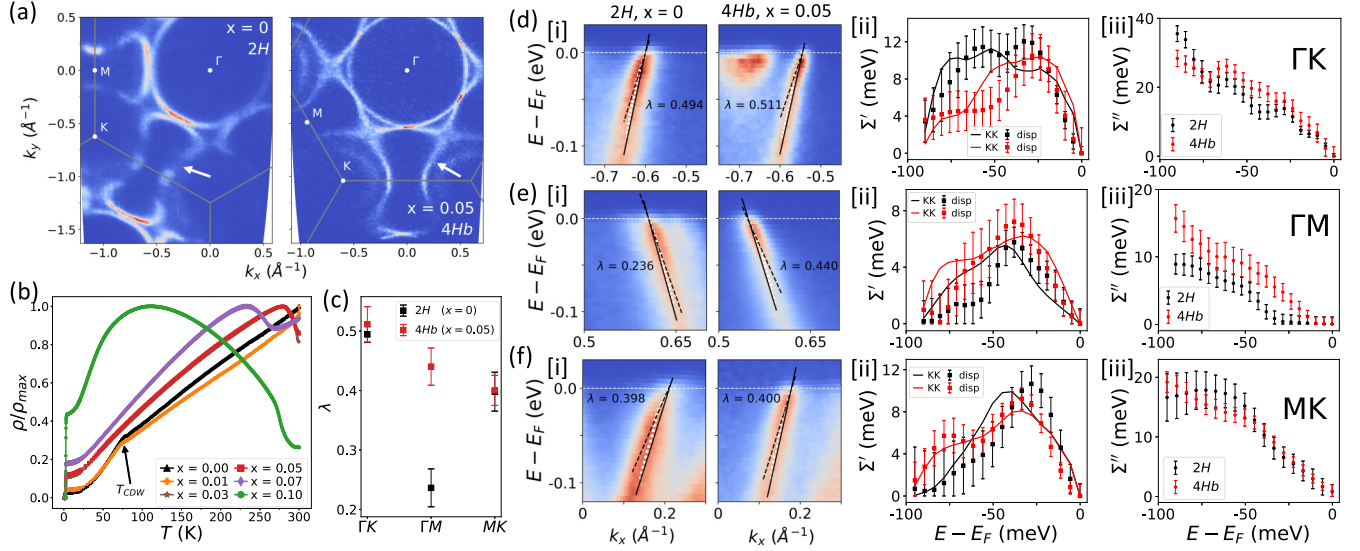
FIG. 4. (a) FSs of $2H$ ($x = 0$, left panel) and $4Hb$ ($x = 0.05$, right panel) samples measured at 18 K. Gapped portions of the $2H$ FS (arrows) are signatures of CDW order. (b) Normalized resistivity measurements as a function of x. A cusp in the resistivity due to the CDW transition at $T \sim 76$ K in the $2H$ phase ($x = 0$ and 0.01) is suppressed in the $4Hb$ phase and other mixed polytypes ($x \geqslant 0.05$). (c) EPC constant λ of the $2H$ ($x = 0$) and $4Hb$ ($x = 0.05$) samples along the Γ-K, Γ-M, and M-K directions. (d) [i] Fitted band dispersion (white squares), as well as the renormalized Fermi velocity (dashed black line) and extracted bare band velocity (solid black line) along the Γ-K direction for the $x = 0$ (right panel) and 0.5 samples (left panel). [ii] ([iii]) Real (imaginary) part of the self-energy, Σ' (Σ''), along the Γ-K direction for $x = 0$ and 0.05. Two methods of computing $\Sigma'(\omega)$ are shown: Kramers-Kronig transformation of $\Sigma''(\omega)$ (KK) and subtraction from the bare band dispersion (disp). Panels (e) and (f) show the same analysis as in panel (d), applied along the Γ-M and M-K directions, respectively.

The FS presented in Fig. 4(a) (left panel) exhibits well-defined gapped regions along the dogbone sheets—clear signatures of a CDW reconstruction. The locations of the gapped portions in the FS sheet (indicated with the white arrows) match those of the sister compound $2H$-TaSe$_2$, where the $q_{CDW} = 2/3|\Gamma - M|$ ordering wave vector leads to a commensurate 3×3 reconstruction of the unit cell [40–42]. Analysis of the Lindhard susceptibility of $2H$-TaS$_2$, included in the SM [29], further establishes the similarities between its CDW state and that of $2H$-TaSe$_2$. Moving from the $2H$ ($x = 0$) system to the $4Hb$ structure ($x = 0.05$), the CDW instability is suppressed, as seen in the right panel of Fig. 4(a). A comparison of the energy distribution curves taken at the k points where the CDW gap opens is included in the SM [29]. The suppression of the CDW phase transition in samples containing a mixture of $2H$ and $1T$ layers ($0.03 \leqslant x \leqslant 0.10$) is confirmed by resistivity measurements, as shown in Fig. 4(b).

In addition, the ARPES data show signatures of electron interactions in the $2H$ band structure in the form of a dispersion "kink" anomaly roughly 30 meV below E_F. The kink can be seen in ARPES dispersion cuts along various momentum directions. It is highlighted by the boxes in Fig. 3(a) and examined in detail in Figs. 4(d)–4(f)[i]. This energetically sharp feature, which has also been noted in previous work [30], ostensibly signals that the electrons couple to a particular boson mode at the same energy. We ascribe the kink to e-ph interactions; calculations of the $2H$-TaS$_2$ phonon band structure find an optical phonon branch with a flat dispersion at the same ∼30-meV scale, where there is substantial EPC over an extended region centered around the Γ-M wave vector [43].

In Figs. 4(d)–4(f), we analyze the dispersion kink to assess changes in the EPC parameter, λ, between the $2H$ ($x = 0$)

and $4Hb$ ($x = 0.05$) samples. We evaluate λ from analysis of the complex electronic self-energy, $\Sigma(\omega) = \Sigma'(\omega) + i\Sigma''(\omega)$, where $\omega = E - E_F$. We follow the general approach of Refs. [44,45], which is based on Lorentzian fitting of the ARPES momentum distribution curves (MDCs) at fixed energies. For each sample, $\Sigma(\omega)$ is analyzed along the Γ-K, Γ-M, and M-K directions. $\Sigma'(\omega)$ and $\Sigma''(\omega)$ are related to the spectra as the difference between the renormalized and noninteracting "bare" dispersions and from the widths of the MDCs at the corresponding energies, respectively. The methodology involves extracting $\Sigma'(\omega)$ by two independent methods—Kramers-Kronig (KK) transformation of $\Sigma''(\omega)$ and analysis of the dispersion (disp)—which self-consistently determine the noninteracting Fermi velocity v_F^0 and thus the absolute scaling of $\Sigma(\omega)$. Details of the calculations and results are described in the SM [29].

The extracted λ values are presented in Fig. 4(c). For the $2H$ phase ($x = 0$), we find λ ranges from 0.236 along the Γ-M direction to 0.494 along the Γ-K direction. This variation in λ is not surprising, as the EPC is known to be k dependent in $2H$-TaS$_2$ [30,46]. It is remarkable, however, that the *enhancement* in EPC in going from the $2H$ phase to the $4Hb$ phase ($x = 0.05$) is strongly momentum dependent. Namely, λ is virtually unchanged at the measured points along the Γ-K and M-K directions, while a large enhancement in the interactions is found along the Γ-M direction, where $\lambda = 0.440$ (an increase of about 85%).

III. DISCUSSION

The results here offer spectroscopic insights into key factors that lead to a strong enhancement of T_c in the mixed-layer

polytypes. The suppression of CDW order restores states to the FS that are especially likely to couple strongly to phonons, allowing them to form Cooper pairs in the competing superconducting phase. Meanwhile the enhancement in EPC at the $\sim$30-meV scale, while strongly momentum anisotropic, is nonetheless substantial in terms of its likely impact on T_c. As an illustration, by applying the McMillan equation [47] and averaging the λ values extracted along the three momentum directions in Figs. 4(d)–4(f), the measured T_c values of 0.8 K and 2.2 K in the $2H$ and $4Hb$ systems, respectively, can be rationalized under reasonable assumptions, even before other factors are taken into account [29].

It follows from this that Mott-like interactions originating from the $1T$ planes should not play a leading role in elevating the T_c in $4Hb$-TaS$_2$. This aligns with the negligible k_z dispersion of the $1T$-FP band within the $4Hb$ system [Fig. 3(b)], as well as the similar U values inferred from DMFT modeling of $1T$ layers in pure and $4Hb$-like systems, which both suggest that Mott interactions remain largely confined within the $1T$ planes. The ARPES measurements furthermore suggest that changes in carrier density, either due to inter- or intralayer charge transfer or doping by the intercalants, probably have little *direct* impact on T_c. Observed changes in the FS volume of the $2H$ bands are too small to account for the large T_c enhancement via the density of states alone and, if anything, would tend to reduce the states at E_F and hence the T_c [28]. Still, small charge transfer and/or doping effects could indirectly influence superconductivity in profound ways, e.g., by altering the *e*-ph interactions.

The strongly momentum-dependent increase in λ highlights the complexity of the interactions in these systems and the need for further study. It is tempting to draw inferences from the fact that we observe a dramatic EPC enhancement at a point in the dispersion along the same momentum direction (Γ-M) as the $2H$ CCDW ordering wave vector. It is possible the the same phonon interactions at play in the CDW order of the $2H$ phase are strengthened and bolster superconductivity in the $4Hb$ system, similar to recent findings in charge-ordered cuprates [33]. Drawing such conclusions, however, will require further studies to the identify the phonon wave vectors where EPC is strongly enhanced.

The observations here may have broader relevance outside of the TaS$_2$ bulk polytypes. Suppression of CDW order and enhancement of EPC were also observed in other intercalated TMDs [48] and atomically thin layers of $2H$-TaS$_2$ [18,19].

The similar behaviors in these systems may be general consequences of isolating individual $1H(')$ layers, which may reduce metallic screening and alter the phonon dispersions and FS nesting conditions.

IV. CONCLUSIONS

In conclusion, using ARPES, we have probed the electronic structures of $2H$-, $1T$-, and $4Hb$-TaS$_2$ in order to investigate the strong enhancement of superconductivity in mixed $2H/1T$ layer polytypes relative to the pure $2H$ structure. Our work utilized vanadium intercalation as a route to synthesize high-quality TaS$_2$ polytypes. The ARPES measurements demonstrate the clear presence of the CDW gap in pure $2H$-TaS$_2$, which by a comparison to isovalent $2H$-TaSe$_2$, might be associated with a commensurate 3×3 reconstruction. ARPES and transport data further show that the CDW is suppressed in mixed $2H/1T$ layer forms of V$_x$TaS$_2$ ($0.03 \leqslant x \leqslant 0.1$). The spectra exhibit a kink dispersion anomaly in the $2H$-derived bands as a signature of energetically sharp electron excitations—presumably *e*-ph interactions—roughly 30 meV below E_F. In the $4Hb$ structure ($x = 0.05$), the EPC associated with the kink is strongly enhanced in a highly momentum-dependent manner. Both the suppression of the CDW and the momentum-anisotropic increase of EPC are likely to be key factors in explaining the large enhancement of T_c when $2H$-TaS$_2$ layers or half-layers are electronically isolated—either as polytypes incorporating $1T$ layers ($4Hb$, $6R$, and other phases), or in monolayer or true heterostructure form.

ACKNOWLEDGMENTS

[1] J. M. E. Harper, T. H. Geballe, and F. J. DiSalvo, Thermal properties of layered transition-metal dichalcogenides at charge-density-wave transitions, Phys. Rev. B **15**, 2943 (1977).

[2] K. Rossnagel, On the origin of charge-density waves in select layered transition-metal dichalcogenides, J. Phys.: Condens. Matter **23**, 213001 (2011).

[3] Y. D. Wang, W. L. Yao, Z. M. Xin, T. T. Han, Z. G. Wang, L. Chen, C. Cai, Y. Li, and Y. Zhang, Band insulator to Mott insulator transition in $1T$-TaS$_2$, Nat. Commun. **11**, 4215 (2020).

[4] M. Klanjšek, A. Zorko, R. Žitko, J. Mravlje, Z. Jagličić, P. K. Biswas, P. Prelovšek, D. Mihailovic, and D. Arčon, A high-

temperature quantum spin liquid with polaron spins, Nat. Phys. **13**, 1130 (2017).

[5] S. Mañas-Valero, B. M. Huddart, T. Lancaster, E. Coronado, and F. L. Pratt, Quantum phases and spin liquid properties of 1T-TaS$_2$, npj Quantum Mater. **6**, 69 (2021).

[6] E. Lahoud, O. N. Meetei, K. B. Chaska, A. Kanigel, and N. Trivedi, Emergence of a novel pseudogap metallic state in a disordered 2D Mott insulator, Phys. Rev. Lett. **112**, 206402 (2014).

[7] T. Ritschel, J. Trinckauf, K. Koepernik, B. Büchner, M. v. Zimmermann, H. Berger, Y. I. Joe, P. Abbamonte, and J. Geck,

Orbital textures and charge density waves in transition metal dichalcogenides, Nat. Phys. **11**, 328 (2015).

[8] W. Li and G. V. Naik, Reorganization of CDW stacking in $1T$-TaS$_2$ by an in-plane electrical bias, APL Mater. **9**, 111103 (2021).

[9] F. Petocchi, C. W. Nicholson, B. Salzmann, D. Pasquier, O. V. Yazyev, C. Monney, and P. Werner, Mott versus hybridization gap in the low–temperature phase of $1T$-TaS$_2$, Phys. Rev. Lett. **129**, 016402 (2022).

[10] A. S. Ngankeu, S. K. Mahatha, K. Guilloy, M. Bianchi, C. E. Sanders, K. Hanff, K. Rossnagel, J. A. Miwa, C. Breth Nielsen, M. Bremholm, and P. Hofmann, Quasi-one-dimensional metallic band dispersion in the commensurate charge density wave of $1T$-TaS$_2$, Phys. Rev. B **96**, 195147 (2017).

[11] Y. Yu, F. Yang, X. F. Lu, Y. J. Yan, Y.-H. Cho, L. Ma, X. Niu, S. Kim, Y.-W. Son, D. Feng, S. Li, S.-W. Cheong, X. H. Chen, and Y. Zhang, Gate-tunable phase transitions in thin flakes of $1T$-TaS$_2$, Nat. Nanotechnol. **10**, 270 (2015).

[12] Y. Liu, Z. Hu, E. Stavitski, K. Attenkofer, and C. Petrovic, Magnetic critical behavior and anomalous Hall effect in $2H - Co_{0.22}TaS_2$ single crystals, Phys. Rev. Res. **3**, 023181 (2021).

[13] H. Liu, S. Huangfu, X. Zhang, H. Lin, and A. Schilling, Superconductivity and charge density wave formation in lithium-intercalated 2H-TaS$_2$, Phys. Rev. B **104**, 064511 (2021).

[14] L. Li, X. Deng, Z. Wang, Y. Liu, M. Abeykoon, E. Dooryhee, A. Tomic, Y. Huang, J. B. Warren, E. S. Bozin, S. J. L. Billinge, Y. Sun, Y. Zhu, G. Kotliar, and C. Petrovic, Superconducting order from disorder in 2H-TaSe$_{2-x}$S$_x$, npj Quantum Mater. **2**, 11 (2017).

[15] Q. Dong, J. Pan, S. Li, Y. Fang, T. Lin, S. Liu, B. Liu, Q. Li, F. Huang, and B. Liu, Record-high superconductivity in transition metal dichalcogenides emerged in compressed 2H-TaS$_2$, Adv. Mater. **34**, 2103168 (2022).

[16] L. J. Li, W. J. Lu, X. D. Zhu, L. S. Ling, Z. Qu, and Y. P. Sun, Fe-doping–induced superconductivity in the charge-density-wave system 1T-TaS$_2$, npj Quantum Mater. **97**, 67005 (2012).

[17] B. Sipos, A. F. Kusmartseva, A. Akrap, H. Berger, L. Forró, and E. Tutiš, From Mott state to superconductivity in 1T-TaS$_2$, Nat. Mater. **7**, 960 (2008).

[18] E. Navarro-Moratalla, J. O. Island, S. Mañas Valero, E. Pinilla-Cienfuegos, A. Castellanos-Gomez, J. Quereda, G. Rubio-Bollinger, L. Chirolli, J. A. Silva-Guillén, N. Agraït, G. A. Steele, F. Guinea, H. S. J. van der Zant, and E. Coronado, Enhanced superconductivity in atomically thin TaS$_2$, Nat. Commun. **7**, 11043 (2016).

[19] Y. Yang, S. Fang, V. Fatemi, J. Ruhman, E. Navarro-Moratalla, K. Watanabe, T. Taniguchi, E. Kaxiras, and P. Jarillo-Herrero, Enhanced superconductivity upon weakening of charge density wave transport in $2H$-TaS$_2$ in the two-dimensional limit, Phys. Rev. B **98**, 035203 (2018).

[20] C. Boix-Constant, S. Mañas Valero, R. Córdoba, J. J. Baldoví, A. Rubio, and E. Coronado, Out-of-plane transport of 1T-TaS$_2$/graphene-based van der waals heterostructures, ACS Nano **15**, 11898 (2021).

[21] M. Mahajan and K. Majumdar, Charge-density wave driven giant thermionic-current switching in 1T-TaS$_2$/2H-TaS$_2$/2H-MoS$_2$ Heterostructure, Adv. Electron. Mater. **8**, 2200866 (2022).

[22] R. Moriya, N. Yabuki, and T. Machida, Superconducting proximity effect in a NbSe$_2$/graphene van der Waals junction, Phys. Rev. B **101**, 054503 (2020).

[23] V. Vaňo, M. Amini, S. C. Ganguli, G. Chen, J. L. Lado, S. Kezilebieke, and P. Liljeroth, Artificial heavy fermions in a van der Waals heterostructure, Nature (London) **599**, 582 (2021).

[24] F. Di Salvo, B. Bagley, J. Voorhoeve, and J. Waszczak, Preparation and properties of a new polytype of tantalum disulfide (4Hb-TaS$_2$), J. Phys. Chem. Solids **34**, 1357 (1973).

[25] A. Ribak, R. Majlin Skiff, M. Mograbi, P. K. Rout, H. M. Fischer, J. Ruhman, K. Chashka, Y. Dagan, and A. Kanigel, Chiral superconductivity in the alternate stacking compound 4Hb-TaS$_2$, Sci. Adv. **6**, eaax9480 (2020).

[26] A. Almoalem, I. Feldman, I. Mangel, M. Shlafman, Y. E. Yaish, M. H. Fischer, M. Moshe, J. Ruhman, and A. Kanigel, The observation of π-shifts in the Little-Parks effect in 4Hb-TaS$_2$, Nat. Commun. **15**, 4623 (2024).

[27] I. Silber, S. Mathimalar, I. Mangel, A. K. Nayak, O. Green, N. Avraham, H. Beidenkopf, I. Feldman, A. Kanigel, A. Klein, M. Goldstein, A. Banerjee, E. Sela, and Y. Dagan, Two-component nematic superconductivity in 4Hb-TaS$_2$, Nat. Commun. **15**, 824 (2024).

[28] A. Almoalem, R. Gofman, Y. Nitzav, I. Mangel, I. Feldman, J. Koo, F. Mazzola, J. Fujii, I. Vobornik, J. Sánchez-Barriga, O. J. Clark, N. C. Plumb, M. Shi, B. Yan, and A. Kanigel, Charge transfer and spin-valley locking in 4Hb-TaS$_2$, npj Quantum Mater. **9**, 36 (2024).

[29] See Supplemental Material at http://link.aps.org/supplemental/10.1103/PhysRevMaterials.8.104802 for further information regarding the experimental, computational, and analytical methods, which includes Refs. [3,14,25,40,41,43–46,49–55], and contains further details about the samples, preparation techniques, measurements, and data analysis.

[30] K. Wijayaratne, J. Zhao, C. Malliakas, D. Young Chung, M. G. Kanatzidis, and U. Chatterjee, Spectroscopic signature of moment-dependent electron–phonon coupling in $2H$-TaS$_2$, J. Mater. Chem. C **5**, 11310 (2017).

[31] F. Clerc, M. Bovet, H. Berger, L. Despont, C. Koitzsch, M. Garnier, and P. Aebi, Charge density waves in 1T-TaS$_2$: An angle-resolved photoemission study, Phys. B: Condens. Matter **351**, 245 (2004).

[32] P. Blaha, Electronic structure and electric field gradients in 2H-TaS$_2$, LiTaS$_2$ and SnTaS$_2$, J. Phys.: Condens. Matter **3**, 9381 (1991).

[33] Q. Wang, K. von Arx, M. Horio, D. J. Mukkattukavil, J. Küspert, Y. Sassa, T. Schmitt, A. Nag, S. Pyon, T. Takayama, H. Takagi, M. Garcia-Fernandez, K.-J. Zhou, and J. Chang, Charge order lock-in by electron-phonon coupling in La$_{1.675}$Eu$_{0.2}$Sr$_{0.125}$CuO$_4$, Sci. Adv. **7**, eabg7394 (2021).

[34] J. Jung, J. W. Park, J. Kim, and H. W. Yeom, Surface enhanced electron correlation on the trivial quasi-two-dimensional bulk insulator 1T-TaS$_2$, Phys. Rev. B **106**, 155406 (2022).

[35] D. Di Sante, P. K. Das, C. Bigi, Z. Ergönenc, N. Gürtler, J. A. Krieger, T. Schmitt, M. N. Ali, G. Rossi, R. Thomale, C. Franchini, S. Picozzi, J. Fujii, V. N. Strocov, G. Sangiovanni, I. Vobornik, R. J. Cava, and G. Panaccione, Three-dimensional electronic structure of the type-II Weyl semimetal WTe$_2$, Phys. Rev. Lett. **119**, 026403 (2017).

[36] Z. Vydrova, E. F. Schwier, G. Monney, T. Jaouen, E. Razzoli, C. Monney, B. Hildebrand, C. Didiot, H. Berger, T. Schmitt, V. N.

Strocov, F. Vanini, and P. Aebi, Three-dimensional momentum-resolved electronic structure of $1T$-TiSe$_2$: A combined soft-x-ray photoemission and density functional theory study, Phys. Rev. B **91**, 235129 (2015).

[37] T. Sato, K. Terashima, S. Souma, H. Matsui, T. Takahashi, H. Yang, S. Wang, H. Ding, N. Maeda, and K. Hayashi, Three-dimensional Fermi-surface nesting in 1T-VSe$_2$ studied by angle-resolved photoemission spectroscopy, J. Phys. Soc. Jpn. **73**, 3331 (2004).

[38] F. Weber, R. Hott, R. Heid, L. L. Lev, M. Caputo, T. Schmitt, and V. N. Strocov, Three-dimensional Fermi surface of $2H-$NbSe$_2$: Implications for the mechanism of charge density waves, Phys. Rev. B **97**, 235122 (2018).

[39] V. N. Strocov, M. Shi, M. Kobayashi, C. Monney, X. Wang, J. Krempasky, T. Schmitt, L. Patthey, H. Berger, and P. Blaha, Three-dimensional electron realm in VSe$_2$ by Soft-X-Ray photoelectron spectroscopy: Origin of charge-density waves, Phys. Rev. Lett. **109**, 086401 (2012).

[40] S. V. Borisenko, A. A. Kordyuk, A. N. Yaresko, V. B. Zabolotnyy, D. S. Inosov, R. Schuster, B. Büchner, R. Weber, R. Follath, L. Patthey, and H. Berger, Pseudogap and charge density waves in two dimensions, Phys. Rev. Lett. **100**, 196402 (2008).

[41] D. S. Inosov, V. B. Zabolotnyy, D. V. Evtushinsky, A. A. Kordyuk, B. Büchner, R. Follath, H. Berger, and S. V. Borisenko, Fermi surface nesting in several transition metal dichalcogenides, New J. Phys. **10**, 125027 (2008).

[42] Y. W. Li, J. Jiang, H. F. Yang, D. Prabhakaran, Z. K. Liu, L. X. Yang, and Y. L. Chen, Folded superstructure and degeneracy-enhanced band gap in the weak-coupling charge density wave system $2H$-TaS$_2$, Phys. Rev. B **97**, 115118 (2018).

[43] N. F. Hinsche and K. S. Thygesen, Electron–phonon interaction and transport properties of metallic bulk and monolayer transition metal dichalcogenide TaS$_2$, 2D Mater. **5**, 015009 (2018).

[44] A. A. Kordyuk, S. V. Borisenko, A. Koitzsch, J. Fink, M. Knupfer, and H. Berger, Bare electron dispersion from experiment: Self-consistent self-energy analysis of photoemission data, Phys. Rev. B **71**, 214513 (2005).

[45] C. H. P. Wen, H. C. Xu, Q. Yao, R. Peng, X. H. Niu, Q. Y. Chen, Z. T. Liu, D. W. Shen, Q. Song, X. Lou, Y. F. Fang, X. S. Liu, Y. H. Song, Y. J. Jiao, T. F. Duan, H. H. Wen, P. Dudin, G. Kotliar, Z. P. Yin, and D. L. Feng, Unveiling the superconducting mechanism of Ba$_{0.51}$K$_{0.49}$BiO$_3$, Phys. Rev. Lett. **121**, 117002 (2018).

[46] C.-S. Lian, C. Heil, X. Liu, C. Si, F. Giustino, and W. Duan, Intrinsic and doping-enhanced superconductivity in monolayer $1H$-TaS$_2$: Critical role of charge ordering and spin-orbit coupling, Phys. Rev. B **105**, L180505 (2022).

[47] W. L. McMillan, Transition temperature of strong-coupled superconductors, Phys. Rev. **167**, 331 (1968).

[48] W. Z. Hu, G. Li, J. Yan, H. H. Wen, G. Wu, X. H. Chen, and N. L. Wang, Optical study of the charge-density-wave mechanism in $2H$-TaS$_2$ and Na$_x$TaS$_2$, Phys. Rev. B **76**, 045103 (2007).

[49] S. F. Meyer, R. E. Howard, G. R. Stewart, J. V. Acrivos, and T. H. Geballe, Properties of intercalated 2H-NbSe$_2$, 4Hb-TaS$_2$, and 1T-TaS$_2$, J. Chem. Phys. **62**, 4411 (1975).

[50] S. Pal, P. Bahera, S. Sahu, H. Srivastava, A. Srivastava, N. Lalla, R. Sankar, A. Banerjee, and S. Roy, Charge density wave and superconductivity in 6R-TaS$_2$, Phys. B: Condens. Matter **669**, 415266 (2023).

[51] H. P. Hughes and R. A. Pollak, Charge density waves in layered metals observed by X-ray photoemission, Philos. Mag. **34**, 1025 (1976).

[52] J. A. Scarfe and H. P. Hughes, Core-level lineshapes in photoemission from transition-metal intercalates of TaS$_2$, J. Phys.: Condens. Matter **1**, 6865 (1989).

[53] J. Laverock, D. Newby, Jr., E. Abreu, R. Averitt, K. E. Smith, R. P. Singh, G. Balakrishnan, J. Adell, and T. Balasubramanian, k-resolved susceptibility function of $2H$-TaSe$_2$ from angle-resolved photoemission, Phys. Rev. B **88**, 035108 (2013).

[54] D. F. Shao, R. C. Xiao, W. J. Lu, H. Y. Lv, J. Y. Li, X. B. Zhu, and Y. P. Sun, Manipulating charge density waves in $1T$-TaS$_2$ by charge-carrier doping: A first-principles investigation, Phys. Rev. B **94**, 125126 (2016).

[55] J. P. Carbotte and F. Marsiglio, Electron-phonon superconductivity, in *The Physics of Superconductors: Vol. I. Conventional and High-T$_c$ Superconductors*, edited by K. H. Bennemann and J. B. Ketterson (Springer, Berlin, 2003), pp. 233–345.